Multiscale Modelling of CO_2 Reduction to Methanol over Industrial $Cu/ZnO/Al_2O_3$ Heterogeneous Catalyst: Linking *ab initio* Surface Reaction Kinetics with Reactor Fluid Dynamics

Andraž Pavlišič*, Matej Huš, Anže Prašnikar and Blaž Likozar

Department of Catalysis and Chemical Reaction Engineering, National Institute of Chemistry, Hajdrihova 19, 1001 Ljubljana, Slovenia

Abstract

There has been a growing trend to couple different levels of modelling, such as going from first-principle calculations to the meso (*e.g.* kinetic Monte Carlo - KMC) and macro scale (*e.g.* computational fluid dynamics - CFD). In the current investigation, we put forward a CFD study of CO_2 hydrogenation to methanol for heterogeneous reacting flows in reactors with complex shape geometries, coupled with first-principle calculations (density functional theory (DFT)). KMC operation simulations were also performed to obtain insight into the uppermost layer conditions during the reaction. With computational fluid dynamics, the focus was placed on the non-uniform catalytic reduction of carbon dioxide to formate, which we treated with a detailed mean-field first-principle microkinetic model, analysed, and corroborated with experiments. The results showed a good consistent agreement with experimental data. The formulated methodological approach paves the way towards full virtual multiscale system descriptions of industrial processing units, encompassing all conventional stages, from catalyst design to the optimisation of mass transfer parameters. Such a bridging is outlined for carbon capture and utilisation.

Keywords: density functional theory (DFT); kinetic Monte Carlo (KMC); computational fluid dynamics (CFD); catalytic reaction microkinetic; hierarchical multiscale modelling

*Correspondence: andraz.pavlisic@ki.si

1. Introduction

Coal and oil are the most common energy resources our society relies upon. Unfortunately, both form in the Slow Carbon Cycle, meaning that their use is an irreversible process for all practical purposes. Moreover, they contribute to the accumulation of CO_2 in the atmosphere. They have been linked to climate change, which is believed to be anthropogenic and caused by increasing levels of the atmospheric CO_2. Although fossil fuel resources are limited, replacing them with cleaner and sustainable substituents is not an easy task due to their importance in the economy. It is crucial that the this problem is addressed proactively (Song, 2006).

The methods of mitigating the greenhouse effect of CO_2 have become a hot topic among researchers in recent years (Change and Impacts, 2003; Haszeldine, 2009; Ni et al., 2018; Wang et al., 2016). An attractive approach is hydrogenation of CO_2 to methanol (Alsayegh et al., 2019; Huff and Sanford, 2011; Martin and Pérez-Ramírez, 2013; Toyir et al., 2001; Van-Dal and Bouallou, 2013). The idea has spread among many fields. For instance, Biernacki et al. showed that by using electricity during surplus production in combination with a wastewater treatment plant, renewable methanol could be produced (Biernacki et al., 2018). Santos et al. screened various potential biogas sources (i.e. landfill, palm oil effluent, corn cobs and sorghum fermentation) and found that the palm oil effluent was presented the highest methanol yield (Santos et al., 2018). From a more theoretical point of view, Moradi et al. showed that sufficient optimization of packed bed reactors for CO_2 hydrogenation could be made with the aid of CFD (Moradi et al., 2014). Nonetheless, carbon utilization (coal-to-methanol) is not considered a renewable process but it is worth mentioning that a significant improvement was made in coal gasification to produce methanol. Highly efficient carbon utilization of coal-to-methanol process integrated with chemical looping hydrogen and air separation technology was shown to be able to drastically reduce the carbon fingerprint (Xiang et al., 2020). As of now, the synthesis of methanol *via* CO_2 hydrogenation seems to be the only feasible process for the fixation of CO_2 on a large scale (Tidona et al., 2013). Moreover, this process is already well established on the industrial scale. Presenting CO_2 as a potential feedstock might instigate the companies dealing with fossil fuels to act as investors in the circular economy (Graciani et al., 2014).

Currently, industrial processes for the production of methanol most commonly use Cu–ZnO/Al_2O_3 (CZA) catalysts at 200-300 ^oC and 50-100 bar with a syngas feed (ARENA et al., 2007; Saito and Murata, 2004; Tidona et al., 2013; Wambach et al., 1999; Yang et al., 2006). These systems suffer from a significant disadvantage: they require relatively high operating temperatures, which limit the theoretical yield of the entropically disfavoured reduction products. Several works reported the development of homogeneous catalysts for the low-temperature conversion of CO_2 to methanol (Huff and Sanford, 2011). However, the industry continues to prefer the CZA catalysts due to their low price, high durability and a favourable ratio between conversion and selectivity. As it is the case with many industrial catalytic processes, the technology for the production preceded the full understanding of the chemical system. Even though the CZA catalysts have been widely studied in the industry for over 40 years, their optimization has relied primarily on empirical knowledge. Thus, the exact mechanism of the reaction pathway and the interplay of the catalytic surface have received much attention in academia in recent years and remain an important research topic.

The questions of synergy between Cu in ZnO (Behrens et al., 2013, 2012; Burch et al., 1990) and the preferable carbon source (CO or CO_2) for methanol remain open (Chinchen et al., 1987; KLIER, 1982). In the quest to establish the exact reaction mechanism and the most effective catalyst, scientists tackle this problem with a theoretical approach. Recent *ab inito* studies of methanol synthesis have provided detailed descriptions of the reaction mechanism on various Cu-based catalysts (Behrens et al., 2012; Grabow and Mavrikakis, 2011; Kattel et al., 2017; Nakatsuji and Hu, 2000; Studt et al., 2013). Several DFT studies confirmed the early work of Chinchen *et al*., who showed that the formate pathway is predominant for the methanol production in a CO_2/CO mixture on these types of catalysts (Chinchen et al., 1987).

An optimal multi-scale linking and integration of atom-scale density functional theory (DFT) computations with meso scale (*e.g.* kinetic Monte Carlo - KMC) and macro scale (*e.g.* computational fluid dynamics - CFD) is gaining importance, particularly when considering the engineering and intensification of unconventional feedstock processing, as well as the design of emerging catalysis routes (Hagman et al., 2018; Kattel et al., 2017; Maestri and Cuoci, 2013; Posada-Borbón et al., 2018; Wu and Yang, 2017). In order to do so, it is mandatory that we understand the reacting system on the atomic scale. Grabow and Mavrikakis presented a comprehensive mean-field microkinetic model for the methanol synthesis and water-gas-shift reactions (Grabow and Mavrikakis, 2011). Despite extensive DFT calculations, their mean-field microkinetic model required some corrections of DFT-calculated values for the results to match the experimental data. In a step forward towards industrial application, Maestri presented the feasibility of coupling mean-field microkinetic model with CFD (Maestri, 2017). In their most recent work Maestri et al. presented CO oxidation on ruthenium oxide, showcasing the capability of the approach in making the multiscale simulation of complex chemical reactors with tabulated KMC model possible (Bracconi and Maestri, 2020). Despite its potential, its applicability has been so far proved only for systems with a limited number of elementary events and species (such as the CO oxidation on metal or oxide surfaces).

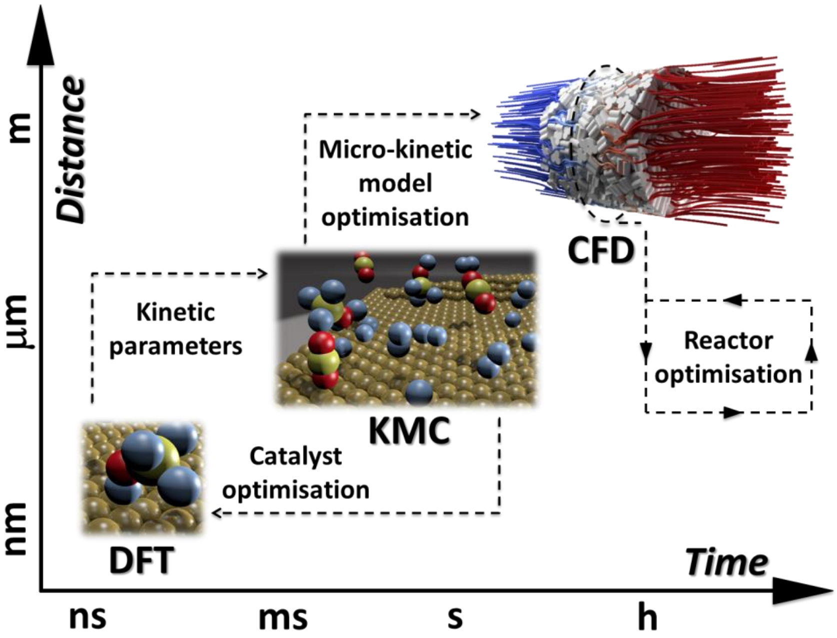

Fig. 1. A general approach to multiscale modelling for real unit engineering.

Although multiscale modelling is a powerful instrumental approach for real unit engineering, fully integrated framework is yet to be developed. Ultimately, it is desirable to obtain a comprehensive description of an operating reactor from the lowest level to the macroscopic scale as shown in Fig. 1. It has become clear from this brief literature review that the existing frameworks are more veraciously described as dual-scale modelling, coupling only two levels together. A further coupling from the smallest scale up to macroscopic transport in a given reactor is still in its infancy, as is any realistic account of the microstructure of real catalysts (Bruix et al., 2019).

In this work, we present a piece of the puzzle towards a fully integrated framework of multiscale modelling of CO_2 hydrogenation to methanol on a commercial Cu-based catalyst.

To the best of our knowledge, the presented work is among the first that put into account all three level (i.e. DFT, KMC and DFT) on a real system process. This is a continuation of our previous work (Huš et al., 2017b), where we obtained first-principle data for the microkinetic scheme. Herein, we present the results of a detailed kinetic Monte Carlo modelling, aimed at elucidating the evolution of the catalyst surface. We show how the surface coverage of different intermediates varies with time and conditions in order to obtain microscopic picture of the catalyst surface. The KMC results were used for the development and implementation of a detailed mean-field first-priciple microkinetic scheme for heterogeneous laminar reacting flows into computational fluid dynamics (CFD). Since some discrepancy between first-principle mean field microkenetic model and experiments was expected, we present a novel approach to overcome this problem *via* single pore approximation. The final results of CFD were consistent with experiments, which proves the feasibility of a fully computational approach to model real system process from catalyst to reactor.

2. The governing equations

Multicomponent mixtures generally require a rather complex convection-diffusion description by the Maxwell-Stefan equations. Due to their high computational cost, simplifications such as the mixture-average approach are often needed (COFFEE and HEIMERL, 1981). For instance, we can assume that all species except one move with nearly the same diffusion velocity, which leads to a Fickian-like description of the diffusion velocity $\boldsymbol{V}_k$:

$$\boldsymbol{V}_k = -\frac{D_{k,m}}{Y_k}\nabla Y_k \,, \qquad [1]$$

where $D_{k,m}$ is the average diffusion coefficient of the k^{th} species mixture and Y_k is the mass fraction. Assuming that the Lewis number (Le_k) equals unity, Eq. 1 simplifies to:

$$\boldsymbol{V}_k = -\frac{\lambda}{Le_k c_P \rho} \nabla Y_k \ , \qquad [2]$$

where c_p is the specific heat capacity of the mixture at constant pressure, ρ is the mixture density and λ is the mixture thermal conductivity. This oversimplification of the convective-diffusion transport can lead to a significant error in the flame velocities and concentration profiles of premixed laminar reacting flames and should be omitted if possible(COFFEE and HEIMERL, 1981). However, in the case of laminar reacting flows in packed bed reactors (PBR), this is still a reasonable assumption.

When axial dispersion and resistance of external/internal mass transport are negligible, the conversion is almost independent of the mass diffusion coefficient, as the main means of transport becomes advection. In other words, the precision in determining $D_{k,m}$ does not affect the accuracy of the result. In practice, this holds true for PBRs operating at high Peclet and low Damköhler numbers (Kamer et al., 2017). To determinate the effect of particle size on the resistance of external/internal mass transport, we prepared samples using crushing and screening of catalyst pellets (see supplementary). We could not observe any significant effect of the particle size on CO_2 conversion, meaning the reactor was operating in the kinetic regime. Moreover, no axial or intermolecular space (space between particles) concentration gradients were observed *via* CFD calculations, which suggests that external mass transfer is negligible. Therefore, we used Eq. 2 to approximate diffusion coefficient, since no special care was needed to describe the diffusion.

2.1. Gas phase

Assuming Newtonian flow, the conservation of global mass, momentum, energy, and the mass of individual species can be summarized as

$$\frac{\partial \rho}{\partial t} + \nabla(\rho \mathbf{v}) = 0 \qquad [3]$$

$$\frac{\partial}{\partial t}(\rho \mathbf{v}) + \nabla(\rho \mathbf{v}\mathbf{v}) = -\nabla p + \nabla \boldsymbol{\tau} \qquad [4]$$

$$\frac{\partial}{\partial t}(\rho Y_k) + \nabla \cdot (\rho Y_k \mathbf{v}) = -\nabla \cdot (\rho Y_k \boldsymbol{V}_k + \dot{r}_k) \qquad [5]$$

$$\frac{\partial}{\partial t}(\rho h_s) + \nabla \cdot (\rho h_s \mathbf{v}) = \nabla \cdot \left(\frac{\lambda}{c_P} \nabla h_s\right) + \frac{\mathrm{D}p}{\mathrm{D}t} + \dot{q}_{reaction} \cdot \qquad [6]$$

In these equations, *t* denotes time, $\boldsymbol{v}$ designates the velocity vector, ρ is the mixture density, $\boldsymbol{\tau}$ is the fluid stress tensor, *p* is the pressure, and $\dot{r}_k$, $\dot{q}_{reaction}$ and h_s are the reaction rates of the *k*th species, the energy source due to reaction and the sensible enthalpy, respectively. The mixture density and transport properties were calculated from the ideal gas law and Sutherland's formula. Since experiment results did not show significant temperature gradient along the reactor, energy equation (eq. 6) was solved without chemical source (see supplementary).

2.2. Surface species

To determine the coverage of surface species site, a detailed mickrokinetic model was developed based on our previous work (Huš et al., 2017b), which we summarise in the next section. The species surface coverages were solved as a set of differential equations, defined as:

$$\frac{\partial \theta_j}{\partial t} = \sum_{i=1}^{nr} S_{ij} r_i \; j = 1, \ldots., NSS \;, \qquad [7]$$

where θ_j is the surface coverage of the j^{th} species, S_{ij} is the "stoichiometric coefficient" (positive for products and negative for reactants), denoting how many times the j^{th} species occurs in the i^{th} reaction, r_i is the elementary reaction rate, *nr* is the number of reactions and *NSS* is the number of the surface species and the number of free surface sites types. As this set of equations is not independent, an additional constraint

$$\sum_{j=1}^{NSS} \theta_j = 1 \qquad [8]$$

must be used in place of one of the Eq. (7) in order to conserve the total number of surface sites.

2.3. Microkinetic model

The question of the preferable carbon source (CO or CO_2) for methanol synthesis is still a matter of speculation and most likely depends upon the catalyst. Therefore, we adopted the reaction pathway for hydrogenation of CO_2 to methanol on industrial Cu/ZnO/Al_2O_3 (CZA) catalyst from our previous work, where a comprehensive reaction network was proposed based on the first-principle DFT calculation, as shown in Fig. 2. Among the most widely studied pathways, reverse water gas shift (RWGS) and formate route (Grabow and

Mavrikakis, 2011; Yang et al., 2010), possible side reactions (i.e. HCOOH-variant of the formate route, CH_2OH formation and hydrogenation of CO) were also considered.

The computational time needed to resolve reacting flows with aid of CFD is highly dependent on the number of elementary reaction steps included in the microkinetic scheme. Therefore, it is desirable to omit any elementary reactions that would lead to dead-ends (e.g. the reaction not proceeding or being too slow due to a high activation energy) or because of a competitive reaction with faster kinetics. In this study, microkinetic scheme was progressively simplified based on the previous results of DFT calculations, KMC simulations (see also next section) and experimental data.

First, all side reactions that lead to HCOOH and CH_2OH formation were eliminated since these products were not detected during the experiments. Second, according to the DFT calculations, the dissociation of HCOO** to HCO* and O* has a prohibitively high activation energy. Third, the KMC simulation was conducted for representative operating conditions of methanol synthesis in the industry (i.e. $T = 500$ K and $P = 40$ bar). The KMC simulation was running until the ergodicity condition was satisfied, meaning that the system was well equilibrated and its time average behaviour corresponded to the space averaged thermodynamic state. For the equilibrated system event frequency analysis was performed for each elementary step, as depicted in Fig. 2, which gives valuable insight into the mechanism and thus provides further indicators for the simplification of the microkinetic scheme.

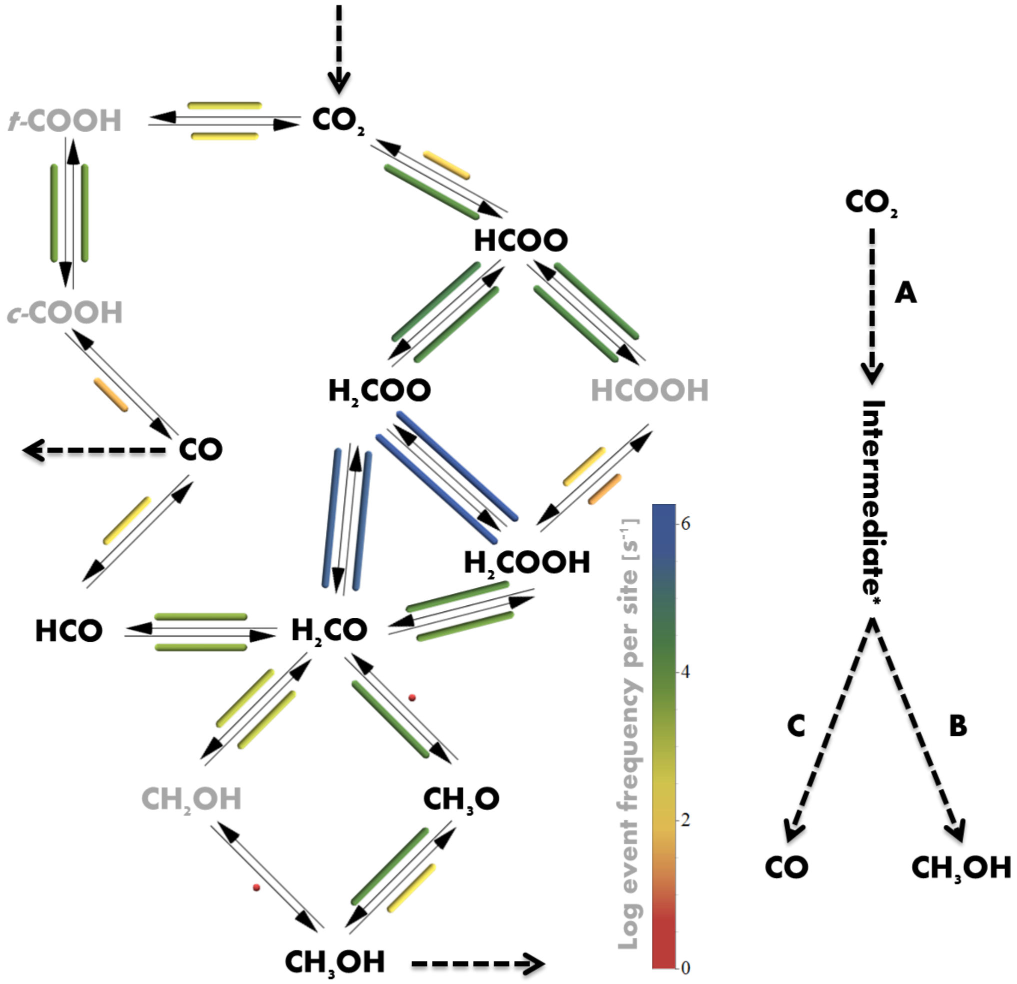

Fig. 2. Left – A scheme of all the considered elementary reaction steps. Colours represent the reaction event frequency (bar length correspond to normalized logarithmic value of reaction event frequency). The intermediates along the most probable route are typeset in bold. Right – A simplified reaction scheme for CO_2 hydrogenation to methanol.

The KMC results irrefutably proved that methanol is produced via the formate route with the following intermediates: HCOO**, H_2COO**, H_2COOH**, H_2CO* and CH_3O*. Firstly, adsorbed or gaseous CO_2 is hydrogenated to HCOO**. HCOO** is further hydrogenated to either HCOOH** or H_2COO**, the letter reaction being more favourable on CZA catalyst (Huš et al., 2017b). Due to a high activation barrier of H_2COO** dissociation (0.81 eV), H_2COO** is next hydrogenated to H_2COOH** (0.32 eV) and then cleaved into H_2CO* and

OH*. Finally, H_2CO* is hydrogenated to CH_2OH* or H_3CO*. However, the event frequency of the latter reaction is a few orders of magnitude higher and thus preferred.

The formation of CO is usually ascribed to the RWGS route, which is an undesired reaction leading to the lower selectivity towards methanol. It is the most important competing reaction, which predominates at higher temperatures (Huš et al., 2017b). However, the KMC simulation indicates that CO is preferentially formed via formate route, which is inconsistent with previous works. The decomposition reaction of c-COOH* to CO* and OH* (RWGS) is 6 times less frequent than dehydrogenation of HCO* (formate route), meaning that majority of CO is essentially a backformation from the H_2CO* intermediate. It should be noted that the preferred route of CO formation is temperature dependent and the RWGS route would eventually prevail over the formate route at higher temperatures. However, herein we focused on the industrial operating conditions of methanol synthesis which usually require temperatures below 550 K (Lange, 2001; Rezaie et al., 2005).

On the basis of previous considerations, we winnow out the most relevant elementary steps for the methanol synthesis. In Fig 2, all intermediate species considered in this study are typeset in bold and their corresponding reactions are summarised in Table 1. The overall reaction model consists of 11 intermediates and five gaseous species, participating in 15 reversible elementary reaction steps (see Table 1). Activation and reaction energies were adopted from our previous work and are labelled next to the corresponding elementary reaction in Table 1 (Huš et al., 2017b).

Despite the fact that DFT gives a solution on the quantum level and thus describes the investigated systems very precisely, the methods harbours several caveats. One of them is directly related to the method itself. There are inherent assumptions within DFT, such as the choice of the exchange correlation functional, the treatment of entropy of the adsorbates etc. For instance, Stud et al. showed the outcome of DFT calculations can be highly dependent on the functional used. They claimed that the highest activation barrier for CO_2 hydrogenation to methanol could vary as much as ~0.4 eV when comparing functionals with or without van der Waals corrections (Studt et al., 2013). However, not all discrepancies between the DFT results and experiments should be assigned to the methodology of first-principle calculations. The model system used in DFT is never a true description of a realistic system. These are too complex (many crystal planes, steps and defects, phase transitions, surface rearrangements etc.) and varied. In specific, Grabow and Masvrikakis showed that even extensive first-principle modelling of methanol production on Cu(111) is inadequate to match the experiments. In the end, they were still resorted to fitting the theoretical input (Grabow and Mavrikakis, 2011).

Nevertheless, DFT is very useful in establishing trends, reaction mechanisms, reaction equilibria and gaining valuable insight into the microscopic behaviour during the reaction. In this work, we resorted to the following constrains for modifying first-principle microkinetic model: (i) finding a minimum set of elementary reactions to describe the observed conversion and selectivity; (ii) adjusting the activation barriers and reaction energy within the accuracy of the DFT calculations (error between 0.2 -0.7 eV for PBE functionals(Maestri, 2017)); (iii) all changes resulting in the same equilibrium state as experimentally measured. With an approach akin to (Grabow and Mavrikakis, 2011), a list of correction factors, as presented in Table 1, were obtained for reactions 4, 7 and 10 (fitting procedure on a single-pore approximation for the PBR showed that altering only kinetic parameters for the three reactions is sufficient to satisfy all the constrains – see section 4.2.3). For details on the calculation of reaction rates (used as input for Eq. 7) from the transition state theory, the reader is referred to our previous work (Huš et al., 2017b).

Table 1: The ZPE-corrected activation energies (E_A) and reaction energies (ΔE) for all elementary steps considered in this study. For this study, these values are adjusted with addition of the correction factors Δ_{Ea} and $\Delta_{\Delta E}$.

i	Elementary reaction	E_a [eV]	Δ_{Ea} [eV]	$\Delta E/\Delta E_{Ad}$ [eV]	$\Delta_{\Delta E}$ [eV]
1	$H_2 + 2* \rightarrow 2\ H*$	0.47	/	-0.13	/
2	$CO_2 + 2* \rightarrow CO_2**$	/	/	-0.23	/
3	$H* + CO_2** \rightarrow HCOO** + *$	0.59	/	-0.65	/
4	$H* + HCOO** \rightarrow H_2COO** + *$	0.90	-0.27	0.32	-0.1
5	$H* + H_2COO** \rightarrow H_2COOH** + *$	0.32	/	-0.23	/
6	$H_2COOH** \rightarrow CH_2O* + OH*$	0.81	/	0.16	/
7	$H* + CH_2O* \rightarrow CH_3O* + *$	0.38	0.038	-0.79	0.153
8	$H* + CH_3O* \rightarrow CH_3OH* + *$	0.46	/	-0.20	/
9	$H* + OH* \rightarrow H_2O* + *$	0.50	/	-0.18	/
10	$H* + HCO* \rightarrow CH_2O* + *$	0.41	-0.164	-0.29	0.087
11	$H* + CO* \rightarrow COH* + *$	1.24	/	0.63	/
12	$CO + * \rightarrow CO*$	/	/	-0.65	/
13	$CH_2OH* \rightarrow CH_3OH + *$	0.72	/	-1.09	/
14	$H_2O + * \rightarrow H_2O*$	/	/	-0.79	/
15[a]	$H* + CO_2 + * \rightarrow HCOO**$	0.25	/	-0.90	/

[a] The kinetic parameters for reaction 15 were taken from Ref (Studt et al., 2015).
Symbol * stands for active site on catalytic surface

3. Methods

3.1. Kinetic Monte Carlo

Kinetic Monte Carlo (KMC) simulations were performed to study the evolution of a catalytic surface. We used the KMC software package Zacros 2.0 (Pineda and Stamatakis, 2017; Stamatakis and Vlachos, 2011a; Vignola et al., 2017), which uses a graph-theoretical implementation of KMC. We define a lattice structure, a reaction mechanism, an energetics model and reaction conditions.

We used a hexagonal lattice with 800 reaction sites. The energetics and reaction mechanism were taken from Ref (Huš et al., 2017b) (see also Table 1). We carried out that the simulations at 200, 220, 240, 260, 280 and 300 °C and 20 bar, and at 1, 10, 20, 30 and 40 bar at 240 °C. The simulations were initialised with an empty lattice and run for $5 \cdot 10^6$ steps, which sufficed for reaching a steady state. We treated very fast steps as quasi-equilibrated. When they reached a quasi-steady state, their forward and reverse reaction rates were slowed down to escape the super basin (Stamatakis and Vlachos, 2011b). For each set of parameters, five simulations with different seeds were performed and averaged for better statics.

3.2. Packing

Beds of the PBR where prepared using the distinct element method (DEM) which simulates realistic packing of the PBR (de Moura Teixeira, 2013; Eppinger et al., 2011; Kuroki et al., 2009; Tabib et al., 2013; Tsory et al., 2013; Vollmari et al., 2015; Wehinger et al., 2015; Zobel et al., 2012). The simulations were conducted with *Blender* (Blender Foundation), which is often used in scientific studies (Boccardo et al., 2015; Icardi et al., 2014; Pavlišič et al., 2018; van Gumster, 2015). It is based on a collection of code, contained in the Bullet Physics Library, used to manage the dynamics of rigid bodies by solving the Newton-Euler equations for both, the translational and rotational motions.

First, five different geometries of catalyst particles were modelled. They were duplicated and scaled to mimic the particle size distribution observed experimentally under a scanning electron microscope (see Fig. 3 and Fig. 8 c). Secondly, randomly distributed and oriented particles in the container above the PBR were allowed to fall freely into the reactor under the gravitational pull. With this technique, we obtain a bed with the following characteristics: (i) height of the bed (h_b) – 10 mm; (ii) ratio between the bed and particle diameter (D_{cut}/d_p) – 5 (iii) numbers of fillers – 1389 (iv) mean particle size – 200 μm (v) porosity – 36.9 %.

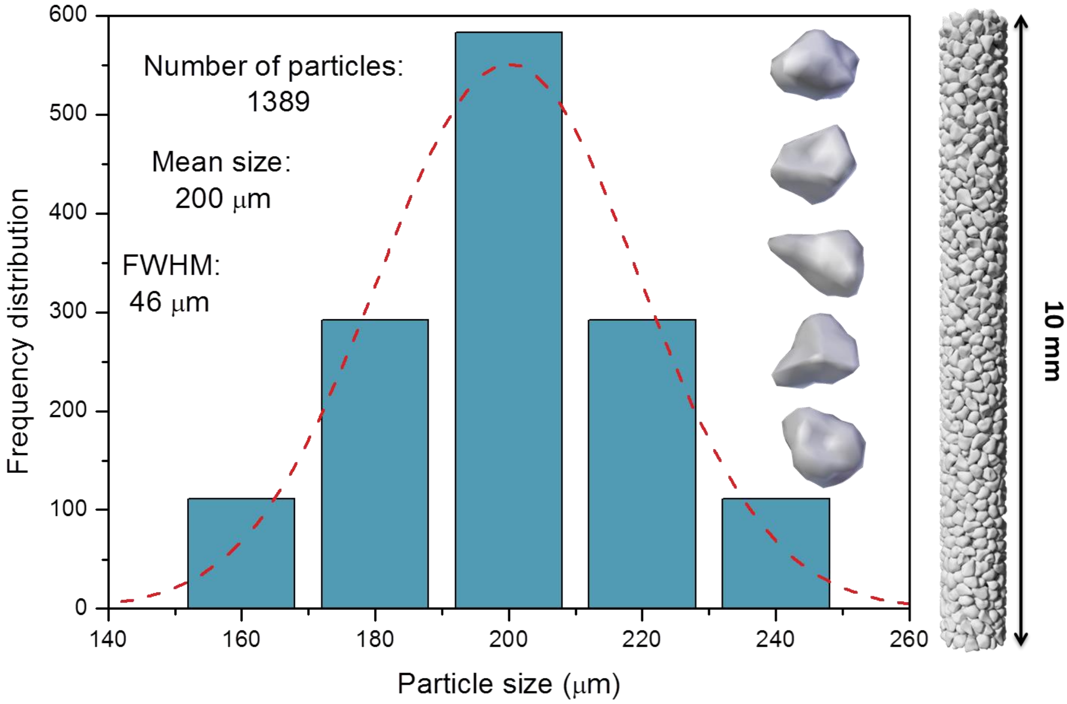

Fig. 3. The characteristics of virtual packing of PBR with arbitrary particles.

3.3. The numerical set-up

In the case of PBR, local phenomena are important to fully understand the chemistry and mass transport inside a chemical reactor (Janardhanan and Deutschmann, 2011). Therefore, it is very important that the computational domain (CD) used in CFD calculations resembles the reactor. However, for high ratios between the reactor diameter (D_r) and the particle diameter (d_p), meshing the whole reactor would require an excessive number of computational cells, resulting in impractically long computational times. Previous studies have shown that it suffices to find a representative cut-segment of the bed ($D_{cut}/d_p > 4$ for arbitrary particles) (Tabib et al., 2013).

In this work, a cylindrical cut-segment (CCG) with the D_{cut}/d_p ratio of 5 was used. As the concentration of species is highly nonlinear along the reactor length, the full height of the catalytic bed was included in the CCG (see Fig. 4 and the experimental section in the supplementary). For meshing, we applied the procedure from our previous work, which proved to be effective in modelling the grid-independent velocity field (Pavlišič et al., 2018). First, a coarse mesh was created. It was then gradually refined with the density profile of the nodes to be finer near the particles/cut-segment walls. Secondly, the bridges between the particles were additionally refined. The final CD consisted of 5 million elements with the average ratio between the particle diameter and the length of mesh cells near the particle surface being 70 (the thickness of the elements layer next to the surface was ~ 3 μm).

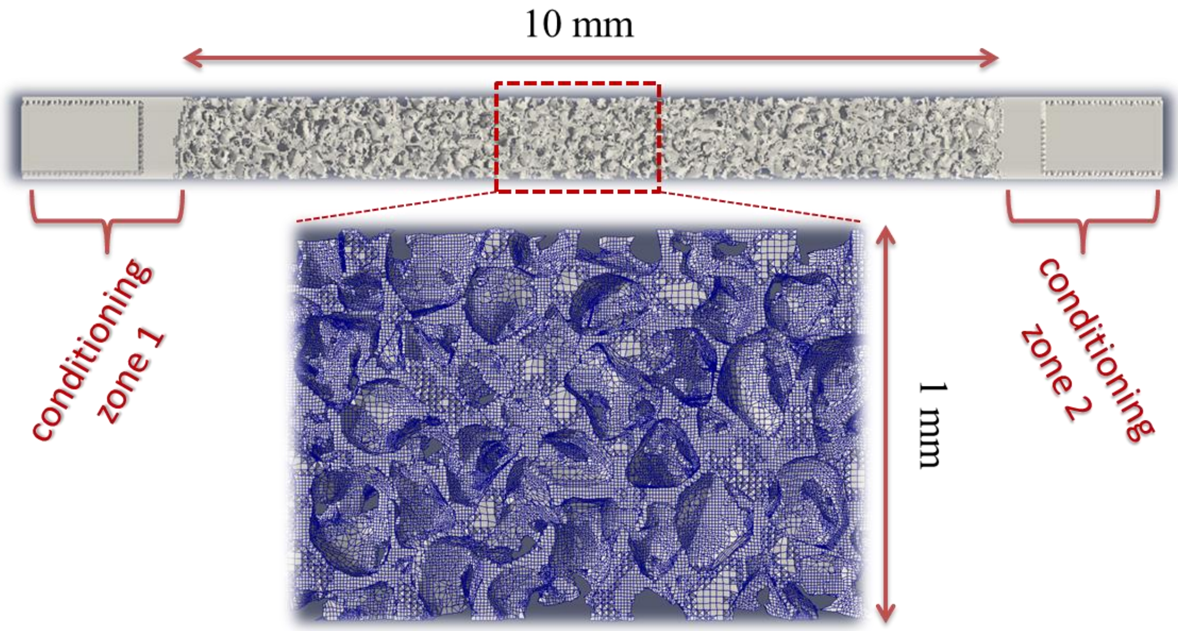

Fig. 4. A cylindrical cut-segment of the catalytic reactor with the corresponding computational mesh.

As we only simulated a CCG, the CFD simulation applies a slip wall boundary condition at the cut-segment surface (zero shear stress boundary condition) and a no-slip boundary condition for the catalytic wall. Since the PBR was operating in isothermal conditions, a fixed temperature was used for all boundaries. The other boundary conditions are, as follows:

- *Cut-segment walls*:

  Zero mass flux for all species:

$$\nabla Y_k|_{cut-segment} = 0 \quad [9]$$

- *Catalytic wall*:

  The mass flux of the individual species *k* is assumed equal to the formation rate due to the heterogeneous reaction occurring at the catalytic wall:

$$\rho D_{k,m}(\nabla Y_k)|_{catalytic} = \alpha_{eff}\dot{r}_k \, , \quad [10]$$

  where α_{eff} is the ratio between the catalytic surface and the geometric area of the bed (*cf.* the next section for calculation details).

- *Inlet/outlet*

  Usually, catalytic reactors require the Danckwerts condition for gas-phase species. In this work, however, a conditioning zone before and after the catalytic bed was added, which reduced the inlet boundary condition to fixed species mass fractions of the initial gas-phase composition. Zero gradients were used for all gas-species for outlet.

Finding a numerical solution for reacting flows represents a challenge since the computational time increases with the number of chemical reactions. Moreover, the relevant ordinary differential equations (ODE) are usually too stiff for first- or second order numerical schemes used in partial differential equations (PDE) for transport phenomena. Therefore, fully-coupled methods considering all processes simultaneously can only be applied to small systems (Maestri and Cuoci, 2013). To overcome this limitation, segregated algorithms based on the operator-splitting methods were developed (Kee and Miller, 1978; Oran and Boris, 2001). With this method, the governing equations are split in sub-equations. Chemical reactions and non-stiff transport equations are thus treated separately.

Herein, we extend the *OpenFoam* solver used for homogenous compressible reacting flows (*reactingFoam*) by adding heterogeneous catalytic reactions (the solver is called *SurfaceReactingFoam*). We were interested only in steady-state, therefore, PDEs were solved by the local time stepping (LTS) algorithm with the second order *LimitedLinear* scheme, while the ODEs were treated by the native Semi-Implicit Bulirsh-Stoer (SIBS) solver. At each iteration of a LTS, firstly momentum equation were solved (step 1 in Fig. 5), followed by calculation of new boundary conditions from Equation 10 by solving the quasi-equilibrium of the surface species coverages (step 2 in Fig. 5). For given fixed partial pressures, the adsorption and desorption rates were determined by solving the ODE of the surface reactions until a steady state was reached. In final stage transport equations were resolved (step 3 in Fig. 5), which close the loop of LTS iteration. The overall solution was considered to be at steady state when the residuals of the pressure and species concentration dropped for 7 and 5 orders of magnitude, respectively.

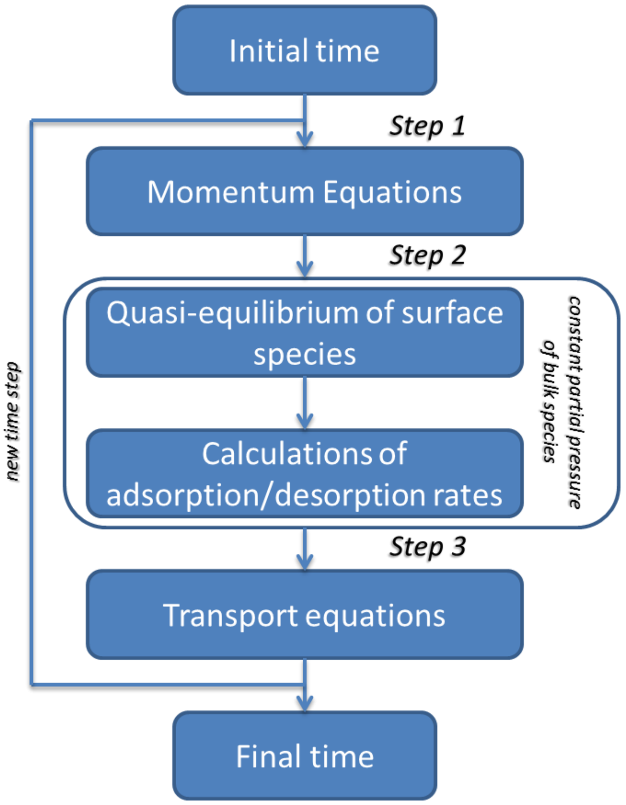

Fig. 5. The numerical algorithm adopted in the *SurfaceReactingFoam* framework.

4. Results and Discussion

4.1. Kinetic Monte Carlo simulations

First, we performed kinetic Monte Carlo simulations to obtain insight into the behaviour of the catalyst surface. In Fig. 6, the surface coverage of a CuZn catalyst is shown at 240 °C and 20 bar. Initially, only hydrogen adsorption takes place until the catalyst surface becomes almost saturated. After 10^{-6} s, the reaction begins to proceed as HCOO** is formed. A steady state is reached after 10^{-2} s. Note that only the most abundant surface species are shown, *i.e.* H*, HCOO**, CH_3OH* and CH_3O*.

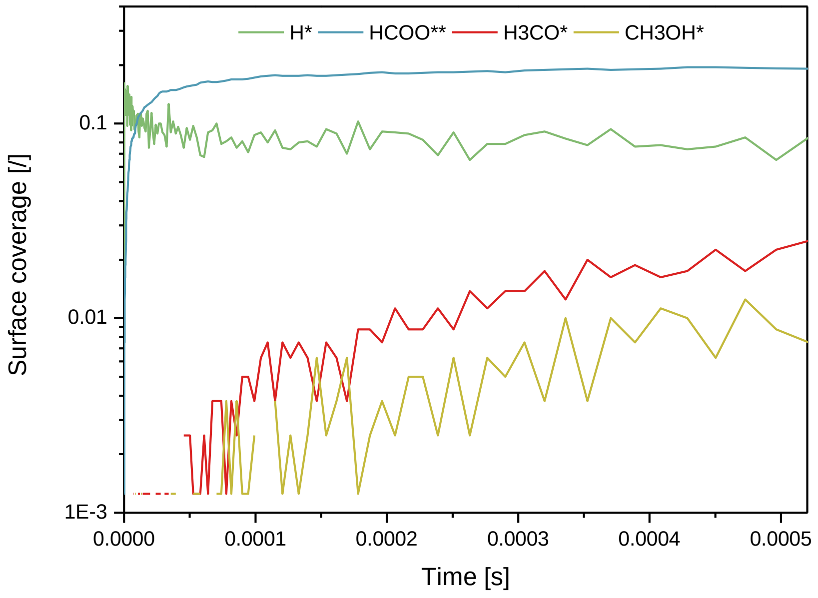

Fig. 6. Time dependence of the surface coverage at 240 °C and 20 bar, as obtained from a KMC simulation.

In Fig. 7, the temperature and pressure dependence of the surface coverage is shown. As the temperature increases, the coverages decrease. The effect is most pronounced for H* intermediate. The coverage of CH_3O* can even slightly increase as it is a late intermediate, whose concentration is strongly dependent on the reaction rate. At low pressures (*i.e.* 1 bar), the coverage of all intermediates is low and increases with the pressure.

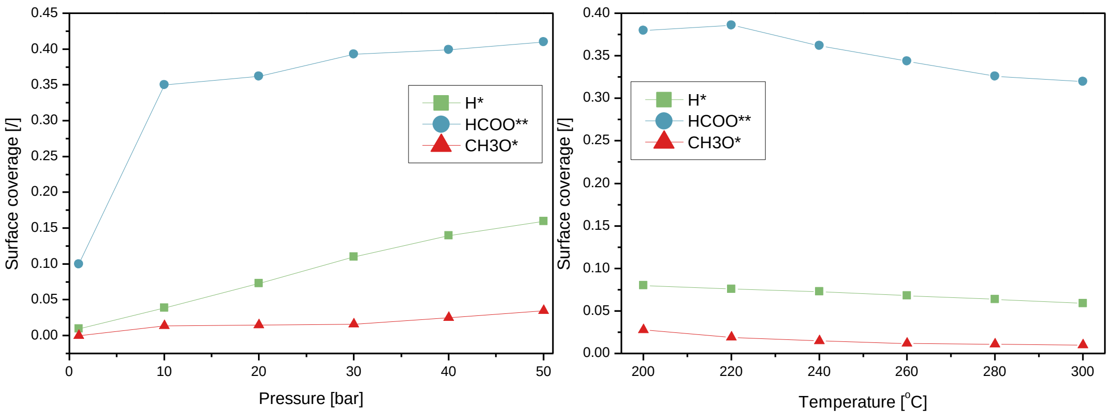

Fig. 7. The surface coverage as obtained from KMC at (left) 240 °C and (right) 40 bar.

4.2. Isothermal CO_2 hydrogenation on a Cu-based industrial catalyst

Having proved that the proposed in-house developed solver *SurfaceReactingFoam* is stable and reliable (see supplementary), we extended its use to a more complex process of CO_2 hydrogenation to methanol on a Cu-based industrial catalyst. First, we fine-tuned the *ab initio* kinetic parameters (from DFT) with the single-pore approximation method. Then, we used the modified kinetic parameters in a realistic virtual PBR that mimics the reactor used in the experiments. With the aid of CFD, CO_2 conversion and selectivity were calculated at various temperatures. The calculations were then compared with the experimental data.

4.2.1. Catalyst characterization

To obtain the necessary parameters for microkinetic modelling, a comprehensive characterisation of Cu-based industrial catalyst was performed. For crystallographic characterisation of its bulk and surface properties, XRD powder diffraction and XPS (X-ray photoelectron spectroscopy) were used. The results presented in Fig. 8 a-b show that bulk and the surface of the catalyst is predominantly composed of a CuO phase. XRD powder diffraction results are consistent with the specification of chemical composition showing that the ratio between CuO and ZnO is approximately 5:3 (since alumina phase was amorphous it could not be detected by XRD powder diffraction). From Rietveld analysis, the crystallite size of CuO and ZnO was calculated to be 6.6 and 4.7 nm, respectively. Morphological characterisation of the catalyst was performed with SEM (scanning electron microscopy) and TEM (transmission electron microscope). Images of TEM and SEM are presented in Fig. 8 cd, which were used to determine the particle shape and particle size distribution (see Section 3.2 Packing). The number of catalytic active sites was determined with the temperature programmed desorption (H_2-TPD) and a Brunauer–Emmett–Teller (BET) surface area measurement, as described in Ref (Huš et al., 2017a) (see Section 4.3.2 for results). Dispersion of copper was measured using dissociative N_2O-chemisorption, as described in Ref (Dasireddy and Likozar, 2017) (see Section 4.3.2).

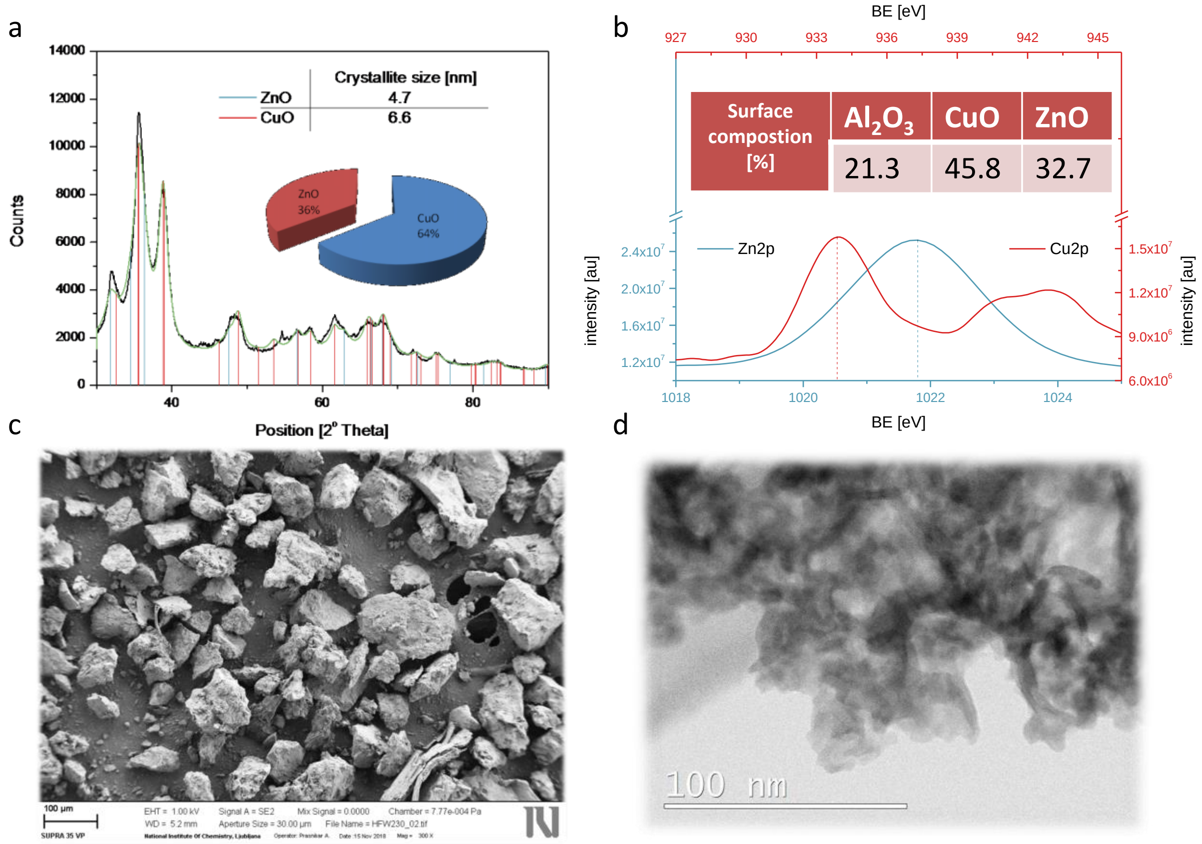

Fig. 8. Catalyst characterization: a) XRD powder diffraction – black line – XRD powder diffraction pattern of the catalyst; green line – Rietveld analysis; red peaks – CuO phase; blue peaks – ZnO phase; b) XPS analysis – on the graph only Cu2p and Zn2p spectra are presented; c) SEM image of the catalyst; d) TEM image of the catalyst.

4.2.2. Determination of the effective catalytic active sites

Most catalysts exhibit a rather complex structure. They may occur as dispersed particles on a flat surface or in a porous substrate. In the case of the Cu-based industrial catalyst for methanol production, the catalyst is synthesised by co-precipitation of hydroxylcarbonate precursors. This results in porous aggregates of strained Cu metal particles, stabilized and promoted by ZnO and Al_2O_3, respectively (Behrens et al., 2013; Girgsdies et al., 2005). The most convenient way to account for such complexity is to relate the catalytic surface area with the geometric surface area by scaling the intrinsic reaction rate at the fluid-solid interphase with two parameters (Janardhanan and Deutschmann, 2011). The first parameter is the ratio between the catalytic surface area and geometric surface area, designated by α_{eff} (see Eq. 10). Its value was determined by the experimentally derived catalytic area with the hydrogen temperature-programmed desorption and the calculated geometrical surface area of the catalytic particles from CD (see Table 2). Secondly, to include the effect of internal mass transfer resistance inside the porous particles, an effectiveness factor (η) was introduced based on the Thiele modulus (Hayes and Kolaczkowski, 1997; Papadias et al., 2000):

$$D_{k,m}(\nabla Y_k)|_{catalytic} = \eta \alpha_{eff} \dot{r}_k \, . \qquad [11]$$

However, for a small Thiele modulus (< 0.1), η approaches unity. In practice this is feasible by reducing the catalyst particle size until the internal mas transfer resistance becomes negligible. Our experiments showed that particles with the size distribution between 160-250 μm are sufficient to supress the internal mas transfer resistance. Therefore, the simplification of the boundary condition from Eq. 10 is a good approximation for modelling reacting flows.

Table 2: Particulate properties of the CAZ catalyst prepared *via* co-precipitation.

Theoretical composition (Cu:Zn:Al)	Surface area (m^2/g)	Cu metal dispersion (%)	Cu metalic surface area (m^2/g)	H_2 chemisorbed (µmol/g)	α_{eff}
50/30/20	96	28	48	31	6500

4.2.3. Fine-tuning of the kinetic parameters by the single-pore approximation

As previously mentioned, the DFT-calculated kinetic parameters can differ from those obtained by experiments. Therefore, fine-tuning of kinetic parameters is necessary for the CFD-modelled reacting flows to reflect experimental data. However, conducting a non-linear regression with CFD for the representative cut-segment of a catalytic PBR would be time consuming. On the other hand, simple continuum-based models, such as the plug flow reactor model (PFR), are fast enough but often too robust. Hence, we developed a single-pore approximation where a PBR is approximated as a monolith converter with square channels. The characteristic dimension of a single channel was calculated as:

$$a_{ch} = \frac{S_{GEO}}{4 \cdot V_{VOID}}, \qquad [11]$$

where a_{ch} is the width of the channel, S_{GEO} is the geometric surface area of the catalyst and V_{VOID} is the void volume of the bed. Additionally, the length of the channel (L_{ch}) was tailored as to mimic the tortuous flow inside the PBR:

$$L_{ch} = h_b \cdot \tau_{PBR}, \qquad [12]$$

where τ_{PBR} is the tortuosity of the PBR, which was adapted from an unstructured sphere packing found in literature (Pavlišič et al., 2018). Finally, the inlet velocity ($v_{ch\text{-}inlet}$) of the channel was calculated as:

$$v_{ch\text{-}inlet} = v_f \cdot \frac{S_{cross}}{A_{pores}} \, . \tag{12}$$

In the equation reported above, v_f is the superficial velocity of the PBR, S_{cut} is the cross-section area of the PBR and A_{pores} is the cross-section area of all channels in a monolith. All boundary conditions needed for the CFD simulation of a single pore were adopted from the PBR (see next section 4.2.4). The characteristic inlet velocity, length and width of the channel were calculated from the parameters reported in Table 3.

Table 3: The parameters needed for the calculation of single-pore dimensions and inlet superficial velocities.

S_{GEO}[mm^2]	porosity [%]	h_b [mm]	τ_{PBR} [/]	S_{cross}[mm^2]	A_{pores}[mm^2]
200	36.9	10	1.2	0.95	0.29

As depicted in the right hand side of Fig. 2, a minimum of three reaction steps are required for the description of adsorption/desorption heterogeneous catalytic reaction of CO_2 hydrogenation. While Reactions B and C are responsible for selectivity, all three reactions contribute to the CO_2 conversion. In theory, tailoring the kinetic parameters of Reaction B and C would be sufficient to reproduce the conversion and selectivity obtained by experiments. However, this could lead to un-physical fitted values of activation and reaction energies since conversion is also restricted by Reaction A. Therefore, three elementary reaction steps were chosen to be fine-tuned in this investigation.

Finding suitable elementary reaction steps for Reactions B and C was straitght-forward since they must share the same intermediate. From Fig. 2, it is evident that this is CH_2O^* with corresponding reactions 7 and 10. On the contrary, Reaction A has four potential candidates (i.e. reaction 3, 4, 5, and 6). Preliminary results showed that the kinetic parameters obtained by DFT resulted in a lower CO_2 conversion than seen in the experiments. Therefore, the elementary reaction step with the lowest equilibrium constants (i.e. reaction 4) was chosen due to the highest potential to push the overall reaction towards the products. Next, for the single pore, the progressive Nelder-Mead algorithm of nonlinear regression was used. The algorithm was iteratively run (with the constrains reported in section 2.3) until the kinetic parameter converged within 1 % of the previous value (the results are summarised in Table 1).

4.2.4. Temperature dependence of the CO_2 conversion and selectivity

In this section, the CFD results for the CO_2 hydrogenation at various temperatures are presented. The computational domain consisted of a CCG with a diameter of 1 mm. The gas mixture of H_2/CO_2 (3:1) with the gas hourly space velocity (GHSV) of 12030 h^{-1} was used as the inlet boundary condition. The reactor was operating at isothermal conditions (200, 220, 240, 260 and 280 ^{o}C) with the constant outlet pressure (20 bar). At the catalytic boundaries, a detailed microkinetic model was applied. In Fig. 9, the final conversion and selectivity for the production of methanol as obtained by CFD are reported. In general, the CFD model is in excellent agreement with the experimental data, showing only minor discrepancies between

220-260 ^{o}C. Both, the CFD and the experimental data show a low CO_2 conversion at low temperature, which gradually increases with temperature. At high temperatures, the conversion of CO_2 asymptotically approaches the thermodynamic equilibrium. Conversely, the selectivity towards methanol is linearly dependent on the temperature, reaching ~80 % at 200 ^{o}C and falling to ~10% at 280 ^{o}C.

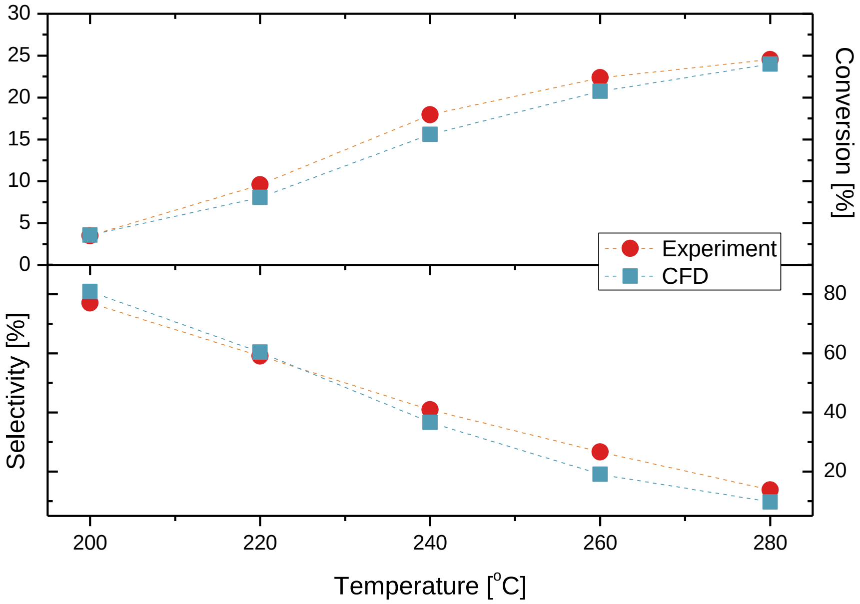

Fig. 9. The temperature dependence of the CO_2 conversion (top) and selectivity towards methanol (bottom) at 20 bars and 12,030 h^{-1} GHSV.

Fig. 10. shows axial cross-sections of the PBR at 220 ^{o}C with the velocity field, CO_2 conversion, selectivity and the surface coverage of methanol. It is apparent that the random structure of packing resulted in a very distorted and non-uniform velocity field with preferential by-pass zones. These strong radial velocity variations result in a non-uniform residence time and could influence the surface reactivity and radial concentration profiles as a consequence (Maestri and Cuoci, 2013).

However, the CO_2 conversion profile shows no variation in radial directions, indicating that the overall reaction rates are limited by kinetics. This also justifies the assumption made in Eq. 2. Since high selectivity and low conversion resulted in nearly constant molar ratio of H_2/CO_2, the selectivity towards methanol shows only minor variations along the PBR. However, there is a large gradient in the methanol surface coverage at the inlet (which is also the case for other adsorbents). Nonetheless, it is quickly smoothed and the reactor operates almost at a constant surface coverage in the last half. In short, this means that even at low temperatures the conversion is restricted by the thermodynamic equilibrium, which is indicative of a PBR with recycle.

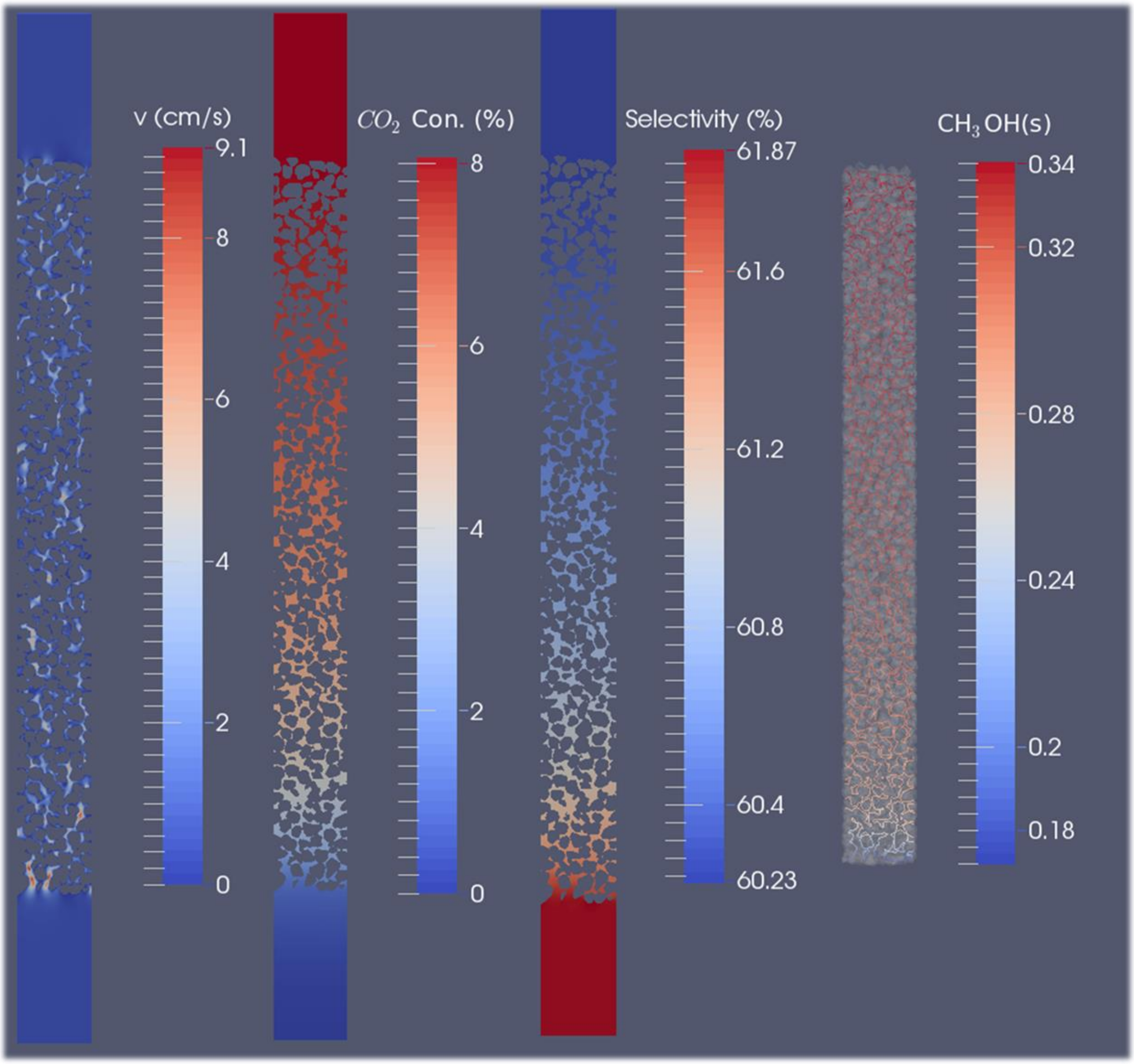

Fig. 10. Cross-sections of the PBR at 220 °C and 20 bar with flow rate of 12,030 h^{-1} GHSV. From left: the velocity field, CO_2 conversion, selectivity towards methanol and surface coverage of methanol.

To get better insight into the large gradients of the surface species coverages, streamlines over a single catalytic particle at the reactor inlet were investigated (Fig. 11). The inlet velocity is significantly lower than that inside the catalytic bed. On average, the velocity inside the PBR is three times higher than the inlet velocity. Consequently, large gradients of the surface species coverages develop because of different resident times of the gaseous species. Special care is needed when designing cooling systems, especially if reaction is fast, as vast amounts of heat would be released at the beginning of the reactor. This finding is consistent with the reports of industrial methanol reactor, where a significant temperature jump was reported at the inlet ($\sim\Delta 20^{o}C$) (Rahimpour et al., 2008; Rezaie et al., 2005). However, a further CFD analysis of the heat transfer is beyond the scope of this work, since experiments were conducted at isothermal condition.

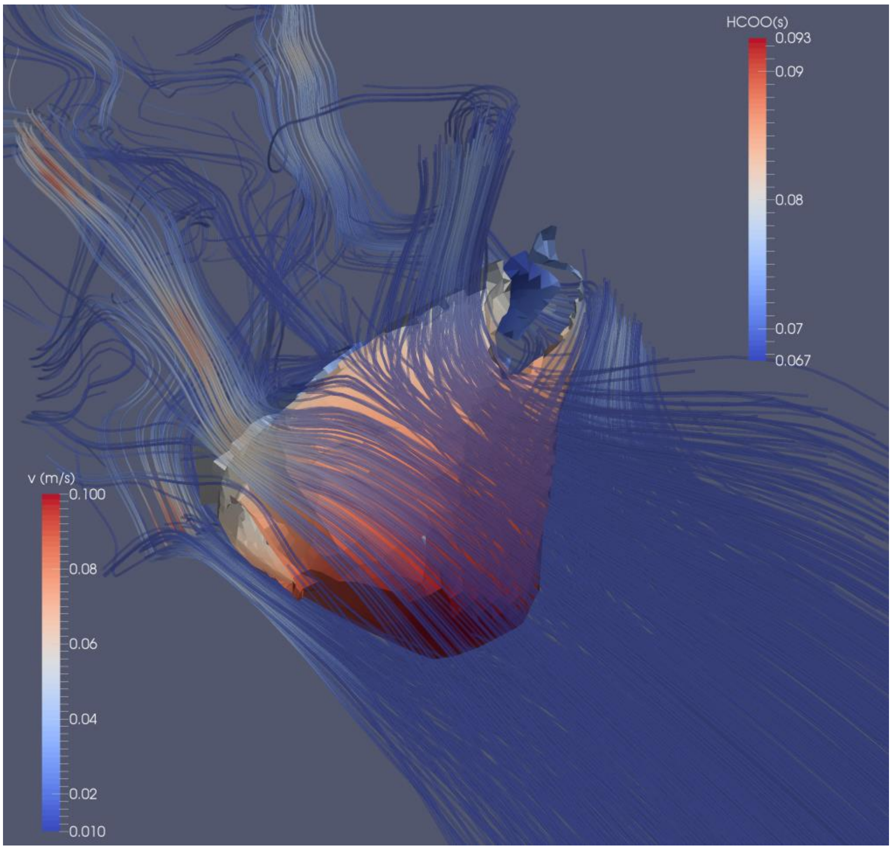

Fig. 11. The velocity field over a single catalytic filler at the reactor inlet (Conditions: 240°C, 20 bar and 12,030 h^{-1} GHSV).

4.2.5. Surface coverage of the most abundant reaction intermediates (MARI)

To show the influence of intermediates on the overall methanol rate production, the surface coverage of the most abundant species is presented in Figs. 12-14. The results are generally consistent with the literature data, showing that formate (HCOO**) and methoxyl (CH_3O*) are the most abundant intermediates (Kattel et al., 2017; Wu and Yang, 2017). This indicates that their production is the bottleneck for the overall reaction. In designing new catalysts, these are the most important species to be considered. Additionally, a substantial amount of water is adsorbed, which is known to act as an inhibitor in methanol synthesis (Saito and

Murata, 2004). This problem could be surmounted with more hydrophobic catalysts, which should boost the overall rate of methanol production.

As already shown, the surface species reach a quasi steady-state in the first 20 % of the reactor since the gas mixture quickly approaches the equilibrium (see Fig. 11). Hence, thermodynamic limitation is an important factor when considering the optimum operational condition and a reactor design for methanol synthesis.

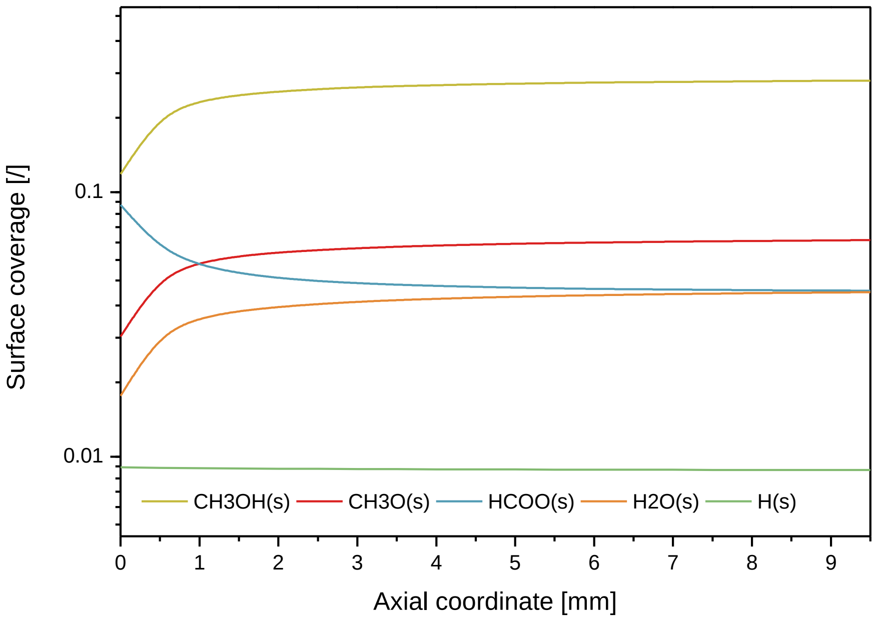

Fig. 12. The axial length dependence of the MARI coverage at 240 ^{o}C and 20 bar.

In Figs. 13-14, the temperature and pressure dependence of MARI is presented. In general, the CFD results are consisted with the KMC simulations, showing that HCOO** and CH_3O* are the most abundant surface species. At low pressure (*i.e.* 1 bar), the surface coverage is low but it steeply increases with pressure (the same trend was observed with KMC). As expected, the surface coverage decreases with increasing temperature. However, a reverse trend was observed for HCOO** and CH_3O* in comparison with KMC. While the surface concentration of HCOO** slightly increases, CH_3O* seems to be strongly dependent on the CH_3OH*

reaction rate. As a consequence, the coverage decreases at higher temperatures. This discrepancy is ascribed to the set-up of the KMC simulations. Since the partial pressure of the reactants was kept constant in KMC, no distinct comparison could be drawn.

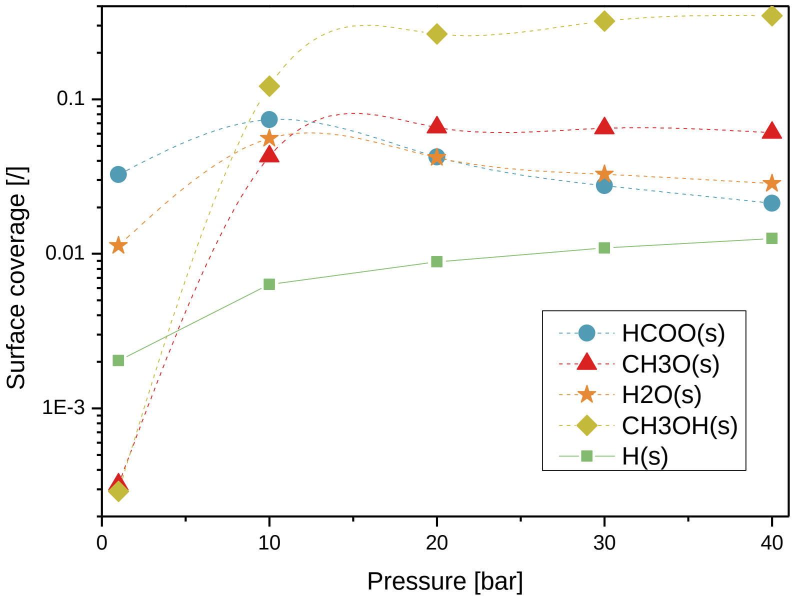

Fig. 13. The pressure dependence of MARI at 220°C.

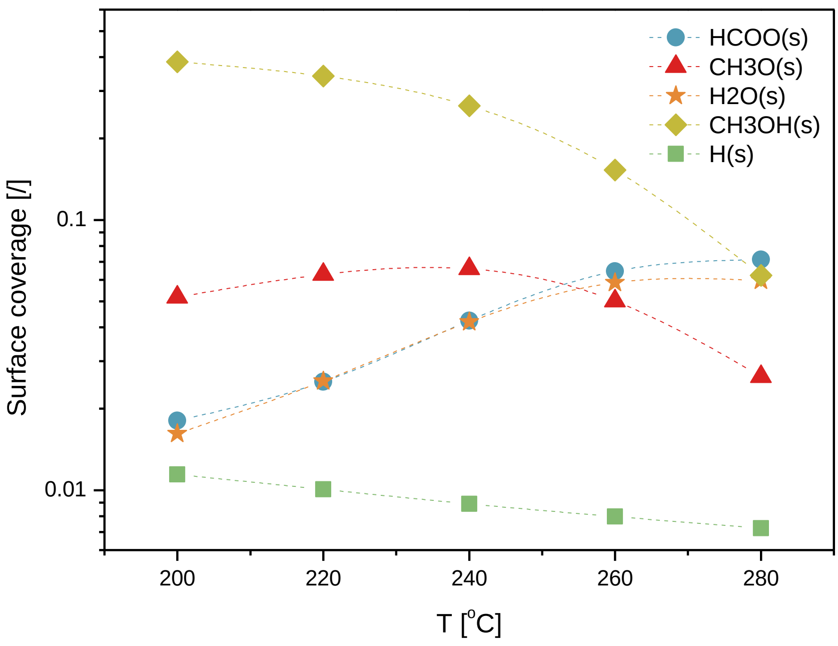

Fig. 14. The temperature dependence of MARI at 20 bar.

4.2.6. Pressure dependence of conversion and selectivity

In this section, the pressure dependence of the conversion and selectivity towards methanol is investigated (Fig. 15). The selectivity towards methanol increases with pressure as a consequence of Le Chatelier's principle. The CFD results are consistent with the thermodynamic equilibrium calculated by STANJAN, which invokes minimizing the appropriate properties (*e.g.* Gibbs or Helmholtz free energy) or maximizing the entropy of the user-supplied gas mixture(“Chemical Equilibrium Calculator,” n.d.).

Looking at the pressure dependence, the CO_2 conversion follows a parabolic relation and reaches the maximum conversion at 10 bar upon attaining the equilibrium. This is the consequence of the constant GHSV: *i.e.* the reactor length is inadequate to reach a full thermodynamic conversion at either high linear velocities due to low pressure *or* high concentrations due to high pressure.

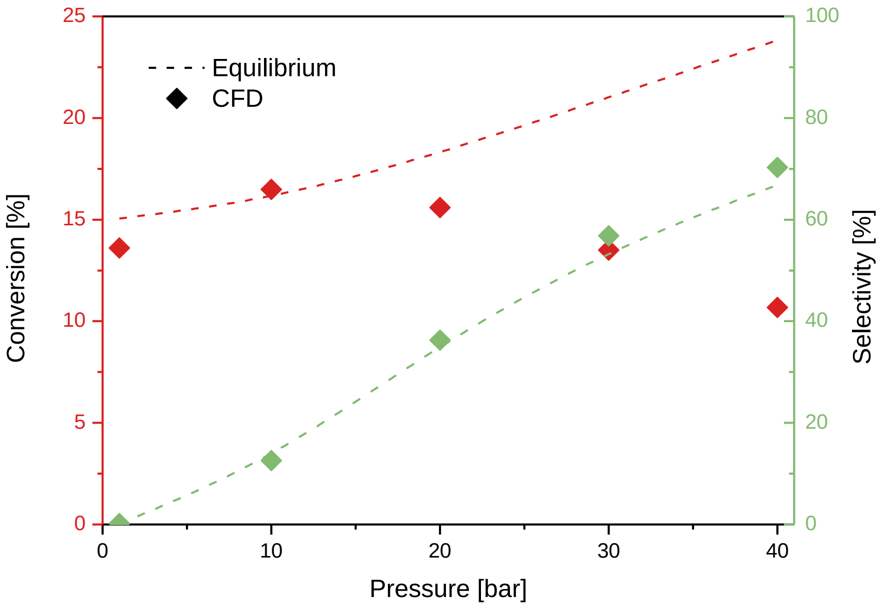

Fig. 15. The pressure dependence of the CO_2 conversion and the selectivity towards methanol at 240 ^{o}C and 12,030 h^{-1} GHSV.

5. Conclusions

In-house solver was developed to solve steady-state heterogeneous reacting flows inside a PBR with complex geometry. The solver *SurfaceReactingFoam* was designed to couple the first-principles kinetics of catalytic chemical reactions with the macroscale Navier-Stokes equations. The proposed solver was implemented within the *OpenFoam* framework and benchmarked against the existing code (*CatalyticFOAM*) with a satisfactory accuracy.

Kinetic Monte Carlo (KMC) simulations were used to show how the catalytic surface coverages change with time and conditions on a microscopic scale. We predict H*, HCOO** and CH_3O* intermediates to be the most abundant surface species. A significant temperature and pressure dependence of the surface species composition was discovered. KMC allowed us to take snapshots and resolve the surface coverage with atomistic detail, which is impossible to achieve with a mean-field approach.

Additionally, a new approach for nonlinear regression of kinetic parameters with the single-pore approximation of the PBR was suggested. First, the most probable reaction route was established from the DFT-calculated potential energy surface, KMC and the transition state theory. A minimum set of kinetic parameters with the highest influence on the conversion and selectivity was chosen with aid of KMC and DFT. In next step they were subjected to further optimization with a two-step minimization procedure. The proposed algorithm combines a minimum set of experiments with a rather small interference of the kinetic parameters obtained by first-principle calculations, which results in a fine-tuned reaction scheme that reflects the experimental data.

Finally, CFD with a detailed first-principle mean-field microkinetic model was conducted for the CO_2 hydrogenation on Cu-based (industrial) catalysts. The modelled conversion and selectivity were consistent with the experiments, which is a big step towards full virtual multiscale modelling of industrial processes. It ranges from catalyst design to the optimisation of process parameters. The CFD coupled with a mean-field first-principle microkinetic model proved as a promising technique for optimizing catalytic reactors. It leads to the final stage of hierarchical modelling where simpler continuous models (such as pseudo-homogeneous PFR) will be coupled with CFD in order to reduce computational time. In this step CFD will provide a tool to calculate empirical parameters which are mandatory for such simplification. All in all, using virtual optimization of catalyst properties, operational conditions and reactor design, costly experimental work can be avoided.

Acknowledgements

The authors gratefully acknowledge the European Commission for partially funding this research with a Horizon 2020 project (ReaxPro: grant agreement N° 814416). The authors also thank the Slovenian Research Agency (ARRS) for funding a core programme P2–0152 and a project J2–7319.

References

Alsayegh, S., Johnson, J.R., Ohs, B., Wessling, M., 2019. Methanol production via direct carbon dioxide hydrogenation using hydrogen from photocatalytic water splitting: Process development and techno-economic analysis. J. Clean. Prod. 208, 1446–1458. doi:10.1016/j.jclepro.2018.10.132

ARENA, F., BARBERA, K., ITALIANO, G., BONURA, G., SPADARO, L., FRUSTERI, F., 2007. Synthesis, characterization and activity pattern of Cu–ZnO/ZrO2 catalysts in the hydrogenation of carbon dioxide to methanol. J. Catal. 249, 185–194. doi:10.1016/j.jcat.2007.04.003

Behrens, M., Studt, F., Kasatkin, I., Kühl, S., Hävecker, M., Abild-Pedersen, F., Zander, S., Girgsdies, F., Kurr, P., Kniep, B.-L., Tovar, M., Fischer, R.W., Nørskov, J.K., Schlögl, R., 2012. The Active Site of Methanol Synthesis over Cu/ZnO/Al2O3 Industrial Catalysts. Science (80-.).

Behrens, M., Zander, S., Kurr, P., Jacobsen, N., Senker, J., Koch, G., Ressler, T., Fischer, R.W., Schlögl, R., 2013. Performance Improvement of Nanocatalysts by Promoter-

Induced Defects in the Support Material: Methanol Synthesis over Cu/ZnO:Al. J. Am. Chem. Soc. 135, 6061–6068. doi:10.1021/ja310456f

Biernacki, P., Röther, T., Paul, W., Werner, P., Steinigeweg, S., 2018. Environmental impact of the excess electricity conversion into methanol. J. Clean. Prod. 191, 87–98. doi:10.1016/j.jclepro.2018.04.232

Boccardo, G., Augier, F., Haroun, Y., Ferr??, D., Marchisio, D.L., 2015. Validation of a novel open-source work-flow for the simulation of packed-bed reactors. Chem. Eng. J. 279, 809–820. doi:10.1016/j.cej.2015.05.032

Bracconi, M., Maestri, M., 2020. Training set design for Machine Learning techniques applied to the approximation of computationally intensive first-principles kinetic models. Chem. Eng. J. 125469. doi:10.1016/j.cej.2020.125469

Bruix, A., Margraf, J.T., Andersen, M., Reuter, K., 2019. First-principles-based multiscale modelling of heterogeneous catalysis. Nat. Catal. doi:10.1038/s41929-019-0298-3

Burch, R., Golunski, S.E., Spencer, M.S., 1990. The role of copper and zinc oxide in methanol synthesis catalysts. J. Chem. Soc. Faraday Trans. 86, 2683. doi:10.1039/ft9908602683

Change, C., Impacts, H., 2003. Climate Change, Human Impacts, and the Resilience of Coral Reefs. Science (80-.). 301, 929–933. doi:10.1126/science.1085046

Chemical Equilibrium Calculator [WWW Document], n.d. URL http://navier.engr.colostate.edu/code/code-4/index.html (accessed 9.13.18).

Chinchen, G.C., Denny, P.J., Parker, D.G., Spencer, M.S., Whan, D.A., 1987. Mechanism of methanol synthesis from CO2/CO/H2 mixtures over copper/zinc oxide/alumina catalysts: use of14C-labelled reactants. Appl. Catal. 30, 333–338. doi:10.1016/S0166-9834(00)84123-8

COFFEE, T., HEIMERL, J., 1981. Transport algorithms for premixed, laminar steady-state flames. Combust. Flame 43, 273–289. doi:10.1016/0010-2180(81)90027-4

Dasireddy, V.D.B.C., Likozar, B., 2017. COx-free hydrogen generation via decomposition of ammonia over copper and zinc-based catalysts. Fuel 196, 325–335. doi:10.1016/j.fuel.2017.01.117

de Moura Teixeira, C.A. de, 2013. Integrated Master in Chemical Engineering.

Eppinger, T., Seidler, K., Kraume, M., 2011. DEM-CFD simulations of fixed bed reactors with small tube to particle diameter ratios. Chem. Eng. J. 166, 324–331. doi:10.1016/j.cej.2010.10.053

Girgsdies, F., Ressler, T., Wild, U., Wübben, T., Balk, T.J., Dehm, G., Zhou, L., Günther, S., Arzt, E., Imbihl, R., Schlögl, R., 2005. Strained thin copper films as model catalysts in the materials gap. Catal. Letters 102, 91–97. doi:10.1007/s10562-005-5208-4

Grabow, L.C., Mavrikakis, M., 2011. Mechanism of Methanol Synthesis on Cu through CO 2 and CO Hydrogenation. ACS Catal. 1, 365–384. doi:10.1021/cs200055d

Graciani, J., Mudiyanselage, K., Xu, F., Baber, A.E., Evans, J., Senanayake, S.D., Stacchiola, D.J., Liu, P., Hrbek, J., Fernández Sanz, J., Rodriguez, J.A., 2014. Highly active copper-ceria and copper-ceria-titania catalysts for methanol synthesis from CO2. Science (80-.). 345, 546–550. doi:10.1126/science.1253057

Hagman, B., Posada-Borbón, A., Schaefer, A., Shipilin, M., Zhang, C., Merte, L.R., Hellman, A., Lundgren, E., Grönbeck, H., Gustafson, J., 2018. Steps Control the Dissociation of CO $_2$ on Cu(100). J. Am. Chem. Soc. jacs.8b07906. doi:10.1021/jacs.8b07906

Hammer, B., Hansen, L.B., Nørskov, J.K., 1999. Improved adsorption energetics within density-functional theory using revised Perdew-Burke-Ernzerhof functionals. Phys. Rev. B - Condens. Matter Mater. Phys. 59, 7413–7421. doi:10.1103/PhysRevB.59.7413

Haszeldine, R.S., 2009. Carbon Capture and Storage: How Green Can Black Be? Science (80-.). 325, 1647–1652. doi:10.1126/science.1172246

Hayes, R.E., Kolaczkowski, S.T., 1997. Introduction to catalytic combustion. Gordon and Breach, Amsterdam.

Huff, C.A., Sanford, M.S., 2011. Cascade Catalysis for the Homogeneous Hydrogenation of CO 2 to Methanol. J. Am. Chem. Soc. 133, 18122–18125. doi:10.1021/ja208760j

Huš, M., Dasireddy, V.D.B.C., Strah Štefančič, N., Likozar, B., 2017a. Mechanism, kinetics and thermodynamics of carbon dioxide hydrogenation to methanol on Cu/ZnAl2O4 spinel-type heterogeneous catalysts. Appl. Catal. B Environ. 207, 267–278. doi:10.1016/j.apcatb.2017.01.077

Huš, M., Kopač, D., Štefančič, N.S., Jurković, D.L., Dasireddy, V.D.B.C., Likozar, B., 2017b. Unravelling the mechanisms of CO 2 hydrogenation to methanol on Cu-based catalysts using first-principles multiscale modelling and experiments. Catal. Sci. Technol. 7, 5900–5913. doi:10.1039/C7CY01659J

Icardi, M., Boccardo, G., Marchisio, D.L., Tosco, T., Sethi, R., 2014. Pore-scale simulation of fluid flow and solute dispersion in three-dimensional porous media. Phys. Rev. E 90, 013032. doi:10.1103/PhysRevE.90.013032

Janardhanan, V.M., Deutschmann, O., 2011. Computational Fluid Dynamics of Catalytic Reactors, in: Modeling and Simulation of Heterogeneous Catalytic Reactions. pp. 251–282. doi:10.1002/9783527639878.ch8

Kamer, P. (Paul C.J.., Vogt, D., Thybaut, J.W., 2017. Contemporary catalysis : science, technology, and applications.

Kattel, S., Ramírez, P.J., Chen, J.G., Rodriguez, J.A., Liu, P., 2017. Active sites for CO 2 hydrogenation to methanol on Cu/ZnO catalysts. Science (80-.). 355, 1296–1299. doi:10.1126/science.aal3573

Kee, R.J., Miller, J.A., 1978. A Split-Operator, Finite-Difference Solution for Axisymmetric Laminar-Jet Biffusion Flames. AIAA J. 16, 169–176. doi:10.2514/3.60873

KLIER, K., 1982. Catalytic synthesis of methanol from CO/H2IV. The effects of carbon dioxide. J. Catal. 74, 343–360. doi:10.1016/0021-9517(82)90040-9

Kuroki, M., Ookawara, S., Ogawa, K., 2009. A High-Fidelity CFD Model of Methane Steam Reforming in a Packed Bed Reactor. J. Chem. Eng. JAPAN 42, s73–s78. doi:10.1252/jcej.08we256

Lange, J.P., 2001. Methanol synthesis: A short review of technology improvements. Catal. Today 64, 3–8. doi:10.1016/S0920-5861(00)00503-4

Maestri, M., 2017. Escaping the trap of complication and complexity in multiscale microkinetic modelling of heterogeneous catalytic processes. Chem. Commun. 53, 10244–10254. doi:10.1039/c7cc05740g

Maestri, M., Cuoci, A., 2013. Coupling CFD with detailed microkinetic modeling in heterogeneous catalysis. Chem. Eng. Sci. 96, 106–117. doi:10.1016/j.ces.2013.03.048

Martin, O., Pérez-Ramírez, J., 2013. New and revisited insights into the promotion of methanol synthesis catalysts by CO2. Catal. Sci. Technol. 3, 3343. doi:10.1039/c3cy00573a

Moradi, F., Kazemeini, M., Fattahi, M., 2014. A three dimensional CFD simulation and optimization of direct DME synthesis in a fixed bed reactor. Pet. Sci. 11, 323–330. doi:10.1007/s12182-014-0347-0

Nakatsuji, H., Hu, Z.-M., 2000. Mechanism of methanol synthesis on Cu(100) and Zn/Cu(100) surfaces: Comparative dipped adcluster model study. Int. J. Quantum Chem. 77, 341–349. doi:10.1002/(SICI)1097-461X(2000)77:1<341::AID-QUA33>3.0.CO;2-T

Ni, Y., Chen, Z., Fu, Y., Liu, Y., Zhu, W., Liu, Z., 2018. Selective conversion of CO2 and H2 into aromatics. Nat. Commun. 9, 3457. doi:10.1038/s41467-018-05880-4

Oran, E.S., Boris, J.P., 2001. Numerical simulation of reactive flow. Cambridge University Press.

Papadias, D., Edsberg, L., Björnbom, P., 2000. Simplified method of effectiveness factor calculations for irregular geometries of washcoats a general case in a 3D concentration field. Catal. Today 60, 11–20. doi:10.1016/S0920-5861(00)00312-6

Pavlišič, A., Ceglar, R., Pohar, A., Likozar, B., 2018. Comparison of computational fluid dynamics (CFD) and pressure drop correlations in laminar flow regime for packed bed reactors and columns. Powder Technol. 328, 130–139. doi:10.1016/j.powtec.2018.01.029

Pineda, M., Stamatakis, M., 2017. Beyond mean-field approximations for accurate and computationally efficient models of on-lattice chemical kinetics. J. Chem. Phys. 147. doi:10.1063/1.4991690

Posada-Borbón, A., Hagman, B., Schaefer, A., Zhang, C., Shipilin, M., Hellman, A., Gustafson, J., Grönbeck, H., 2018. Initial oxidation of Cu(100) studied by X-ray photo-electron spectroscopy and density functional theory calculations. Surf. Sci. 675, 64–69. doi:10.1016/j.susc.2018.04.015

Rahimpour, M.R., Khosravanipour Mostafazadeh, A., Barmaki, M.M., 2008. Application of hydrogen-permselective Pd-based membrane in an industrial single-type methanol reactor in the presence of catalyst deactivation. Fuel Process. Technol. 89, 1396–1408. doi:10.1016/j.fuproc.2008.06.013

Rezaie, N., Jahanmiri, A., Moghtaderi, B., Rahimpour, M.R., 2005. A comparison of homogeneous and heterogeneous dynamic models for industrial methanol reactors in the presence of catalyst deactivation. Chem. Eng. Process. Process Intensif. 44, 911–921. doi:10.1016/j.cep.2004.10.004

Saito, M., Murata, K., 2004. Development of high performance Cu/ZnO-based catalysts for methanol synthesis and the water-gas shift reaction. Catal. Surv. from Asia 8, 285–294. doi:10.1007/s10563-004-9119-y

Santos, R.O. dos, Santos, L. de S., Prata, D.M., 2018. Simulation and optimization of a methanol synthesis process from different biogas sources. J. Clean. Prod. 186, 821–830. doi:10.1016/j.jclepro.2018.03.108

Song, C., 2006. Global challenges and strategies for control, conversion and utilization of CO2 for sustainable development involving energy, catalysis, adsorption and chemical processing. Catal. Today 115, 2–32. doi:10.1016/J.CATTOD.2006.02.029

Stamatakis, M., Vlachos, D.G., 2011a. A graph-theoretical kinetic Monte Carlo framework for on-lattice chemical kinetics. J. Chem. Phys. 134. doi:10.1063/1.3596751

Stamatakis, M., Vlachos, D.G., 2011b. Equivalence of on-lattice stochastic chemical kinetics with the well-mixed chemical master equation in the limit of fast diffusion. Comput. Chem. Eng. 35, 2602–2610. doi:10.1016/j.compchemeng.2011.05.008

Studt, F., Abild-Pedersen, F., Varley, J.B., Nørskov, J.K., 2013. CO and CO2 Hydrogenation to Methanol Calculated Using the BEEF-vdW Functional. Catal. Letters 143, 71–73. doi:10.1007/s10562-012-0947-5

Studt, F., Behrens, M., Kunkes, E.L., Thomas, N., Zander, S., Tarasov, A., Schumann, J., Frei, E., Varley, J.B., Abild-Pedersen, F., Nørskov, J.K., Schlögl, R., 2015. The Mechanism of CO and CO 2 Hydrogenation to Methanol over Cu-Based Catalysts. ChemCatChem 7, 1105–1111. doi:10.1002/cctc.201500123

Tabib, M. V., Johansen, S.T., Amini, S., 2013. A 3D CFD-DEM Methodology for Simulating Industrial Scale Packed Bed Chemical Looping Combustion Reactors. Ind. Eng. Chem. Res. 52, 12041–12058. doi:10.1021/ie302028s

Tidona, B., Koppold, C., Bansode, A., Urakawa, A., Rudolf von Rohr, P., 2013. CO2 hydrogenation to methanol at pressures up to 950bar. J. Supercrit. Fluids 78, 70–77. doi:10.1016/j.supflu.2013.03.027

Toyir, J., Ramírez de la Piscina, P., Fierro, J.L.G., Homs, N., 2001. Catalytic performance for

CO2 conversion to methanol of gallium-promoted copper-based catalysts: influence of metallic precursors. Appl. Catal. B Environ. 34, 255–266. doi:10.1016/S0926-3373(01)00203-X

Tsory, T., Ben-Jacob, N., Brosh, T., Levy, A., 2013. Thermal DEM–CFD modeling and simulation of heat transfer through packed bed. Powder Technol. 244, 52–60. doi:10.1016/j.powtec.2013.04.013

van Gumster, J., 2015. Blender for dummies, 3rd ed. John Wiley & Sons Inc., New Jersey.

Van-Dal, É.S., Bouallou, C., 2013. Design and simulation of a methanol production plant from CO2 hydrogenation. J. Clean. Prod. 57, 38–45. doi:10.1016/j.jclepro.2013.06.008

Vignola, E., Steinmann, S.N., Vandegehuchte, B.D., Curulla, D., Stamatakis, M., Sautet, P., 2017. A machine learning approach to graph-theoretical cluster expansions of the energy of adsorbate layers. J. Chem. Phys. 147. doi:10.1063/1.4985890

Vollmari, K., Oschmann, T., Wirtz, S., Kruggel-Emden, H., 2015. Pressure drop investigations in packings of arbitrary shaped particles. Powder Technol. 271, 109–124. doi:10.1016/j.powtec.2014.11.001

Wambach, J., Baiker, A., Wokaun, A., 1999. CO2 hydrogenation over metal/zirconia catalysts. Phys. Chem. Chem. Phys. 1, 5071–5080. doi:10.1039/a904923a

Wang, S., Li, Q., Fang, C., Zhou, C., 2016. The relationship between economic growth, energy consumption, and CO2 emissions: Empirical evidence from China. Sci. Total Environ. 542, 360–371. doi:10.1016/j.scitotenv.2015.10.027

Wehinger, G.D., Eppinger, T., Kraume, M., 2015. Detailed numerical simulations of catalytic fixed-bed reactors: Heterogeneous dry reforming of methane. Chem. Eng. Sci. 122, 197–209. doi:10.1016/j.ces.2014.09.007

Wu, P., Yang, B., 2017. Significance of Surface Formate Coverage on the Reaction Kinetics of Methanol Synthesis from CO 2 Hydrogenation over Cu. ACS Catal. 7, 7187–7195.

doi:10.1021/acscatal.7b01910

Xiang, D., Li, P., Yuan, X., Cui, P., Huang, W., 2020. Highly efficient carbon utilization of coal-to-methanol process integrated with chemical looping hydrogen and air separation technology: Process modeling and parameter optimization. J. Clean. Prod. 258. doi:10.1016/j.jclepro.2020.120910

Yang, C., Ma, Z., Zhao, N., Wei, W., Hu, T., Sun, Y., 2006. Methanol synthesis from CO2-rich syngas over a ZrO2doped CuZnO catalyst. Catal. Today 115, 222–227. doi:10.1016/j.cattod.2006.02.077

Yang, J., Wang, Q., Zeng, M., Nakayama, A., 2010. Computational study of forced convective heat transfer in structured packed beds with spherical or ellipsoidal particles. Chem. Eng. Sci. 65, 726–738. doi:10.1016/j.ces.2009.09.026

Zobel, N., Eppinger, T., Behrendt, F., Kraume, M., 2012. Influence of the wall structure on the void fraction distribution in packed beds. Chem. Eng. Sci. 71, 212–219. doi:10.1016/j.ces.2011.12.029

Graphical abstract


CO2 + H2
=
CH3OH + H2O